

MIT Open Access Articles

Bright Excitonic Fine Structure in Metal-Halide Perovskites: From Two-Dimensional to Bulk

The MIT Faculty has made this article openly available. **Please share** how this access benefits you. Your story matters.

Citation: Bright Excitonic Fine Structure in Metal-Halide Perovskites: From Two-Dimensional to Bulk. Katarzyna Posmyk, Natalia Zawadzka,, Mateusz Dyksik, Alessandro Surrente, Duncan K. Maude, Tomasz Kazimierczuk, Adam Babiński, Maciej R. Molas, Wakul Bumrungsan, Chanisara Chooseng, Watcharaphol Paritmongkol, William A. Tisdale, Michał Baranowski, and Paulina Plochocka. *Journal of the American Chemical Society* 2024 146 (7), 4687-4694.

As Published: 10.1021/jacs.3c11957

Publisher: American Chemical Society

Persistent URL: <https://hdl.handle.net/1721.1/164754>

Version: Final published version: final published article, as it appeared in a journal, conference proceedings, or other formally published context

Terms of use: Creative Commons Attribution



Bright Excitonic Fine Structure in Metal-Halide Perovskites: From Two-Dimensional to Bulk

Katarzyna Posmyk, Natalia Zawadzka, Łucja Kipczak, Mateusz Dyksik, Alessandro Surrente, Duncan K. Maude, Tomasz Kazimierczuk, Adam Babiński, Maciej R. Molas, Wakul Bumrungras, Chanisara Chooseng, Watcharaphol Paritmongkol, William A. Tisdale, Michał Baranowski,* and Paulina Plochocka*



Cite This: *J. Am. Chem. Soc.* 2024, 146, 4687–4694



Read Online

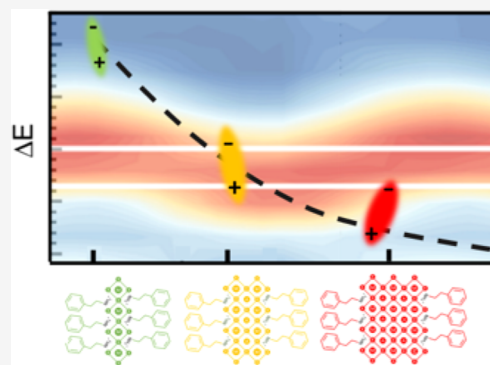
ACCESS |

Metrics & More

Article Recommendations

Supporting Information

ABSTRACT: The optical response of two-dimensional (2D) perovskites, often referred to as natural quantum wells, is primarily governed by excitons, whose properties can be readily tuned by adjusting the perovskite layer thickness. We have investigated the exciton fine structure splitting in the archetypal 2D perovskite $(\text{PEA})_2(\text{MA})_{n-1}\text{Pb}_n\text{I}_{3n+1}$ with varying numbers of inorganic octahedral layers $n = 1, 2, 3,$ and 4 . We demonstrate that the in-plane excitonic states exhibit splitting and orthogonally oriented dipoles for all confinement regimes. The evolution of the exciton states in an external magnetic field provides further insights into the g -factors and diamagnetic coefficients. With increasing n , we observe a gradual evolution of the excitonic parameters characteristic of a 2D to three-dimensional transition. Our results provide valuable information concerning the evolution of the optoelectronic properties of 2D perovskites with the changing confinement strength.



INTRODUCTION

Excitons represent fundamental (interband) electronic excitation in a semiconductor. The role of this Coulomb-bound electron–hole pair is particularly important for quantum confined systems, where electrostatic and exchange interactions are enhanced, strongly affecting the transitions' energy spectrum and the selection rules.^{1–7} Therefore, a detailed understanding of the excitonic properties of such nanostructures is crucial to their use in optoelectronic and photonic devices. For decades, confined systems served as platforms to investigate fundamental exciton physics.^{1,8–12} Recently, two-dimensional (2D) van der Waals crystals^{13–16} have remarkably enriched this excitonic playground, essentially due to the combined spatial and dielectric confinement effects, which are particularly strong. A beautiful illustration of this is given by 2D metal-halide perovskites,^{14,17,18} where tightly bound excitons (with exciton binding energy reaching several hundred meV) open the path to investigate light–matter interaction in a strong coupling regime far above cryogenic temperatures^{19,20} or considerably pronounced exciton fine structure.^{3,6,21,22}

In 2D perovskites, the degeneracy of excitonic states with respect to the angular momentum is often completely lifted,^{3,5,6,24} due to enhanced exchange interactions and the low lattice symmetry. The fine structure splitting (FSS) of excitonic states can reach values of a few up to tens of meV.^{3,4,6,25} This is orders of magnitude larger than in “classical” III–V semiconductor nanostructures,^{1,11,26} making

2D perovskites a very attractive medium to study^{3–6,22,25,27–29} and (potentially) use the exciton fine structure.^{30–32}

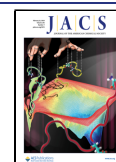
The structure of 2D perovskites can be seen as natural quantum wells, where slabs of metal-halide octahedral units are surrounded from both sides by large organic cations, as schematically shown in Figure 1a. 2D perovskites form type-I quantum wells, where charge carriers are confined in the octahedral slab, and the organic spacers act as the barrier, which provides both spatial and dielectric confinement.^{14,33,34} Such organic–inorganic stacks, belonging to the Ruddlesden–Popper phase of the 2D perovskite subgroup,^{14,17} are described by the general formula $\text{L}_2\text{A}_{n-1}\text{M}_n\text{X}_{3n+1}$, where L is a large organic monovalent cation, A is a small monovalent cation, M is a metal atom, X is a halide atom, and n denotes the number of octahedral layers. The exciton binding energy in 2D perovskites can reach several hundreds of millielectronvolts for the thinnest quantum wells ($n = 1$) and can be decreased to as low as several meV when tuning between the 2D and three-

Received: October 26, 2023

Revised: January 26, 2024

Accepted: January 26, 2024

Published: February 7, 2024



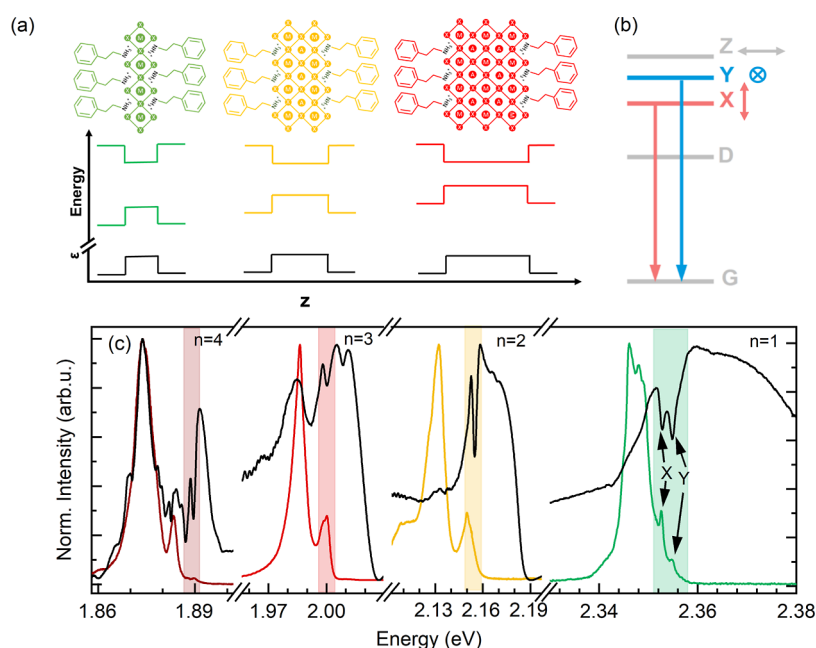


Figure 1. (a) Schematic view of a single layer of 2D perovskites with $n = 1, 2, 3$ inorganic layers, together with the band alignment and dielectric screening profile, which provide quantum and dielectric confinement. (b) Scheme of the band-edge exciton fine structure for $\text{PEA}_2(\text{MA})_{n-1}\text{Pb}_n\text{I}_{3n+1}$ 2D perovskites. G denotes a ground state of the system (no exciton) and X and Y are the linearly polarized orthogonal states relevant to this work; Z and D complete the exciton manifold, where D = dark state, and Z = bright state polarized out of the plane of the crystal. (c) Photoluminescence (PL) (colored lines) and reflectance (black lines) spectra for samples with varying thicknesses of inorganic layers— n . Shaded areas indicate the excitonic transitions. For $n = 1$, the arrows indicate the two in-plane bright exciton states. The multiple resonance structures visible in the reflectance spectra for $n = 3$ and $n = 4$ are attributed to the phonon replica of the main excitonic transition. A more detailed discussion can be found in the [Supporting Information](#).

dimensional (3D) limits by controlling the quantum well thickness.^{18,21,35–37}

In metal-halide perovskites, we can distinguish four band-edge exciton states, which differ in their total angular momentum, and their out-of-plane projection, namely, a bright triplet and dark singlet state.^{7,38–40} The exchange interaction between the spins of the electrons and holes always splits the bright states and dark exciton states. Depending on the symmetry of the system, the degeneracy of the bright states can be either partially or completely lifted.^{7,40,41} In the latter case, the dipoles of the three split bright states are linearly and orthogonally polarized. The fine structure of the ground exciton state is schematically presented in [Figure 1b](#). This excitonic fine structure has been experimentally established for the orthorhombic phase of bulk and perovskite nanocrystals^{7,12,32,38,42,43} as well as in the 2D perovskite $(\text{PEA})_2\text{PbI}_4$.^{3–6,22,24}

It is perhaps surprising that, despite the easy tunability, the impact of the quantum confinement on the exciton fine structure in 2D perovskites has not been investigated so far, even though it appears to be crucial to understand the high emission efficiency of these materials.^{4,38,44} This is even more intriguing, considering that the FSS of bright exciton states has already been observed in bulk metal-halide perovskites,²³ revealing the evolution of the electronic properties between the two extrema of the quantum confinement regime ($n = 1$ and $n = \infty$). It is noteworthy that the quantitative understanding of the evolution of the excitonic structure is not straightforward. The increase in the inorganic layer thickness not only alters the quantum confinement but is also coupled with changes in dielectric conditions and carrier mass.^{18,35} Consequently, a

robust experimental benchmark is crucial for developing any exciton theory bridging the gap between 2D and 3D limits.

Here, we address this challenge by focusing on the bright (in-plane) exciton fine structure in archetypal 2D perovskite $(\text{PEA})_2(\text{MA})_{n-1}\text{Pb}_n\text{I}_{3n+1}$ (where PEA stands for phenylethylammonium and MA stands for methylammonium), often referred to as PEPI. With the use of polarization-resolved and magneto-optical spectroscopy, we investigated the evolution of the bright in-plane exciton state splitting as a function of the inorganic octahedral layers' thickness ($n = 1, \dots, 4$). We find that the in-plane state splitting systematically decreases with increasing n , reaching the value expected for bulk perovskites already for $n = 4$. We further determine the evolution of the bright exciton g -factors, which also systematically approach the bulk values with increasing quantum well thickness. The extracted parameters can be used as a benchmark for the band structure and exciton state modeling because they contain information concerning the anisotropy and dispersion of the bands.

RESULTS

The investigated high-quality $(\text{PEA})_2(\text{MA})_{n-1}\text{Pb}_n\text{I}_{3n+1}$ ($n = 1, \dots, 4$) crystals were grown by a cooling-induced crystallization method^{45,46} with an average crystal size of a few millimeters ([Figure S1](#)). The high phase purity of these crystals was confirmed by powder X-ray diffraction ([Figure S2](#)), which shows clean diffraction patterns of their respective phases. Optical spectra, namely, microphotoluminescence (μPL) and microreflectance (μR) were taken in the backscattering geometry at temperature $T = 4.2$ K. The measurements were performed using an objective having a numerical aperture (NA) of 0.55, selectively sensitive to the states with an in-plane

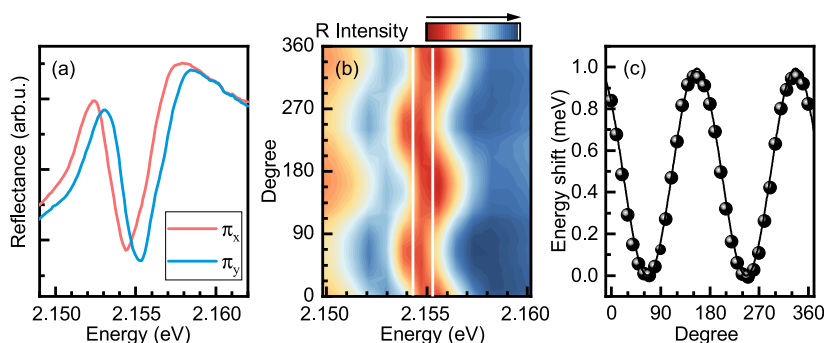


Figure 2. (a) Reflectance spectra measured from the sample with $n = 2$ in two orthogonal linear polarizations showing clear splitting between the two in-plane bright states of the exciton fine structure. Results for samples with $n = 3$ and $n = 4$ are shown in the Supporting Information. (b) Dependence of the reflectance spectrum for PEPI $n = 2$ versus polarization angle. White lines indicate the energies of the two states. (c) The energy difference between the two features in reflectance extracted with a differential method is described in detail in reference 23²³ and Supporting Information. The black line is a $\cos^2(x)$ fit to the data points.

orientation. Typical spectra of PL and reflectance (R) measured from the samples with $n = 1, \dots, 4$ are shown in Figure 1c. With increasing n , the PL spectrum and exciton resonances (indicated by shaded areas) visible in the reflectance spectra shift toward lower energies—an indication of decreasing quantum and dielectric confinement.^{18,35} We notice that for all samples, the PL spectra show a complex line shape with two main features. The dominating PL features are red-shifted with respect to the resonant excitonic features of reflectance spectra, while the less intense PL peaks overlap with them (shaded areas in Figure 1b). Based on aligning of high-energy PL peaks with the excitonic transitions observed in reflectance spectra, we attribute them to the free exciton recombination³ (see also a more extended discussion presented in the Supporting Information). At the same time, the more intense, red-shifted PL peak can be attributed to local potential variation, related to shallow trap states,⁴⁷ to band gap fluctuation,^{48,49} or to polaronic effects.^{50,51} Evidently, the relaxation processes are faster than the free exciton recombination, because in each sample, the PL is dominated by a low-energy part related to excitons trapped at extrinsic defects^{47,51–53} or local lattice reconfiguration.^{48–50,54} The detailed origin of the complex PL spectrum is beyond the scope of this work. From now on, we focus on the analysis of the reflectivity response, which unequivocally probes the energy associated with free excitonic transitions.

For the case of $(\text{PEA})_2\text{PbI}_4$ (thinnest quantum well, $n = 1$), the significant splitting (~ 2 meV) of the two in-plane (X and Y) states has been already reported^{3,6,22,29} and is easily observed both in the reflectance and PL spectra even without the use of polarization optics, as shown in Figure 1c (indicated by the arrows). For the remaining three samples ($n = 2, 3$, and 4), to reveal the FSS of the bright exciton, we performed polarization-resolved reflectance measurements.

Two reflectance spectra taken with two orthogonal linear polarizations π_X and π_Y for sample $n = 2$ are presented in Figure 2a. Similar spectra for the thicker 2D perovskites are shown in the Supporting Information (Figures S3–S5). The energy shift of the transition between the π_X and π_Y polarizations (red and blue curve) is the signature of bright exciton FSS,^{3,6,23} hidden in nonpolarization-resolved spectra, due to the broadening of the transitions. We then performed a full angular dependence of the reflectance spectra versus polarization angle shown in Figure 2b and observed the characteristic oscillating pattern with a 180° period, resulting

from the varying contribution of the two orthogonally polarized excitonic states with slightly different energy. To precisely determine the value of the FSS, we analyze the shift of the resonance versus the analyzer angle. To accurately extract the small-energy shift, we use the method described in detail in the SI and in the literature.^{23,55} The energy shift dependence ΔE is shown in Figure 2c. It is well-fitted with the function $\Delta E = \delta \cos^2(\alpha + \phi)$, where α is the detection angle, ϕ is the phase, and $\delta = 1.0$ meV (for $n = 2$ sample) is the bright in-plane exciton FSS.

We applied the same procedure for the remaining crystals. The value of bright exciton FSS splitting δ versus the thickness of the quantum well is summarized in Figure 3 (red circles)

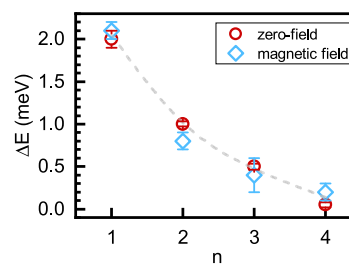


Figure 3. Energy splitting as a function of the number of inorganic octahedron layers n , extracted from polarization-resolved measurements without the magnetic field (circles) and from magneto-optical measurements (diamonds).

and Table 1. The energy spacing between the in-plane excitonic states δ systematically decreases from ~ 2 to ~ 0.2 – 0.1 meV with increasing n . This can be qualitatively

Table 1. Summary of the Parameters Extracted from the Measurements in the Magnetic Field^a

n	δ (meV)		g_{\parallel}	c_0 ($\mu\text{eV}/\text{T}^2$)
	$B = 0$	$B \neq 0$		
1	2 (0.1)	2.1 (0.1) ³	1.2 ²¹	0.36 ²¹
2	1 (0.03)	0.8 (0.1)	2.1	1.25
3	0.5 (0.04)	0.4 (0.2)	2.23	1.7
4	0.05 (0.03)	0.2 (0.1)	2.4	2.2

^aValues of the energy splitting taken from the polarization-resolved measurements at zero field and extracted from the fitting with eq 3. Values in brackets are uncertainty estimations from fits.

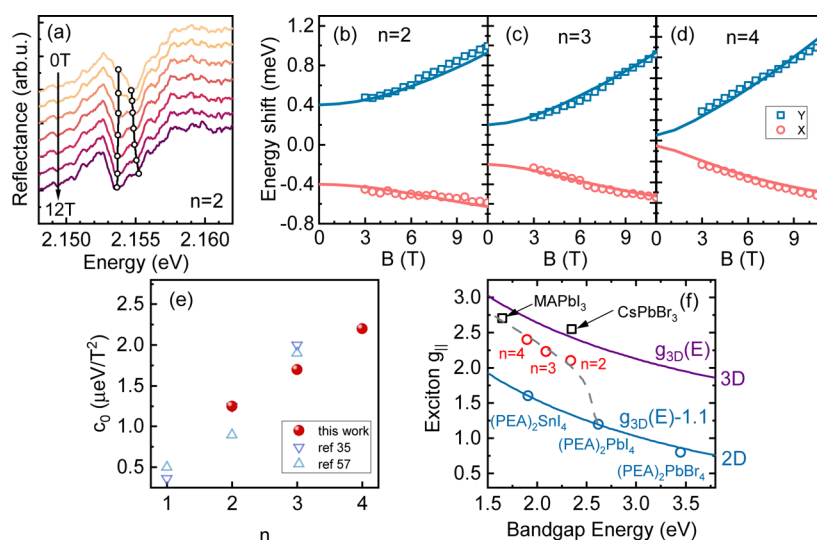


Figure 4. (a) Reflectance spectra for the $n = 2$ sample at different magnetic fields. Black lines track the shift of the excitonic transition as a function of the magnetic field. Results for samples with $n = 3$ and $n = 4$ are shown in the Supporting Information. Energy of the bright excitonic in-plane states with respect to the magnetic field for (b) $n = 2$, (c) $n = 3$, and (d) $n = 4$ samples. (e) Diamagnetic coefficient as a function of the number of inorganic octahedron layers n . Values obtained in references 35 and 57 are displayed for comparison. (f) Exciton g -factor in the direction parallel to the c axis of the crystal as a function of the band gap energy. Values of the bulk perovskite $g_{3D}(E)$ are taken after reference 58,⁵⁸ and values of g -factors for 2D perovskites are taken after reference 4.⁴ The gray dashed line is a guide to the eye showing the evolution of g -factors from the 2D limit to the bulk limit.

understood as the result of the decreasing exciton binding energy and the related increase of the extension of the exciton wave function in wider quantum wells.³⁵ The increased distance between the electron and hole reduces the exchange interaction, which results in a decreasing bright exciton FSS.^{2,26,42,56} On a quantitative level, the provided values can serve as a benchmark for exciton models in metal-halide perovskites. For instance, for $n = 4$, the extracted $\delta \approx 0.1$ meV is comparable to the expected value for the bulk perovskite crystal (100–200 μeV ^{2,23,43}).

To gain a deeper insight into the observed excitonic states, we measured the magnetoreflectance spectrum in the Faraday configuration ($B \parallel k \parallel c$) in static magnetic fields up to 12 T at temperatures $T \approx 10$ K. As shown in Figure 4a, the magnetic field increases the splitting between the in-plane excitonic states. The observed evolution of the transition energy as a function of the magnetic field provides an additional measure of δ as well as exciton g -factor and diamagnetic shift.^{1,3,23,36,41} In the Faraday configuration, in-plane bright excitonic states are mixed with each other, gradually changing from linearly polarized at zero field to circularly polarized at high magnetic field.^{1,23} This effect is nicely visible in Figure 4a, where we show our measurements in the magnetic field on a circular polarization basis. At zero field, bright states are linearly polarized, therefore both are visible in the spectrum. However, with increasing field, as they gain a finite degree of circular polarization, one of the states becomes more prominent in one polarization (see also Figure S6 in the Supporting Information).

The energy $E_{Y/X}$ of each exciton state X and Y in the presence of the exchange interaction and the magnetic field is described by

$$E_{Y/X}(B) = \frac{1}{2}[(E_Y + E_X) \pm \sqrt{\delta^2 + g_B^2 \mu_B^2 B^2}] + c_0 B^2 \quad (1)$$

where B is the magnetic field, μ_B is the Bohr magneton, and g_B is the bright exciton g -factor along the c -axis of the crystal given by the sum of the electron and hole g -factors

$$g_B = g_e \parallel + g_h \parallel \quad (2)$$

c_0 is the diamagnetic coefficient, which depends on the size of the exciton wave function.³⁵ The opposite shifts (\pm) of X and Y transitions arise from the Zeeman effect.^{1,23,41} The transition-energy shift relative to the average energy of in-plane excitonic transition ($\frac{1}{2}(E_Y + E_X)$) at zero field is

$$\Delta E_{Y/X}(B) = \pm \frac{1}{2} \sqrt{\delta^2 + g_B^2 \mu_B^2 B^2} + c_0 B^2 \quad (3)$$

The evolution of the shift of the excitonic states in the magnetic field for samples $n = 2, 3$, and 4 (for a detailed analysis see Supporting Information) is summarized in Figure 4b–d (the dependence for $n = 1$ has already been published³). In the analysis, we omit the spectra below 3 T because excitonic states for samples $n = 3$ and 4 cannot be resolved very accurately at low fields. By fitting the data with eq 3, we extract the values of δ , c_0 , and g_B as a function of n . The dependence of $\delta(n)$ obtained with this approach is shown in Figure 3. We emphasize that the values extracted with the two different approaches (energy dependence on the magnetic field and linear polarization-resolved measurements at 0 field) are in very good agreement, further confirming the validity of our analysis.

The non-negligible influence of the diamagnetic shift is also visible in the presented data. The blue shift and the red shift of the upper and lower energy transitions are not symmetric, which reflects the quadratic term in eq 3. The extracted diamagnetic shift coefficients c_0 increase with n , due to the increasing in-plane extension of the exciton wave function in thicker quantum wells³⁵ ($c_0 \sim \langle r^2 \rangle$ where $\langle r^2 \rangle$ is a mean-square wave function extension⁵⁹). The values of c_0 are shown

together with previously reported values^{35,57} in Figure 4e, and they show very good agreement with each other.

Our measurements also allow us to obtain the dependence of the bright exciton g -factors as a function of n . This is shown in Figure 4 (f) (red circles), together with the g -factors for other representatives of 3D (black squares) and 2D perovskites (blue circles).^{4,21,60–62} The values of the exciton g -factor for $n = 2, 3$, and 4 are exactly between the 2D ($n = 1$) and 3D cases and gradually approach the 3D value (MAPbI₃), which points to a crucial influence of the confinement on the g -factor. The observed variation in the exciton g -factor aligns with the broad predictions of the k - p model for metal-halide perovskites.^{58,60} Consistent with expectations, the values of the g -factor decrease with the opening of the band gap. It is worth noting that the evolution of the g -factor as a function of the band gap shows the same curvature for 3D and 2D perovskites ($n = 1$). To illustrate this, we plot the k - p model prediction for the exciton g -factor in 3D perovskites after reference 58⁵⁸ as a purple line. The same line, shifted downward by 1.1, perfectly describes the g -factors in PEA-based 2D perovskites (blue line). The change of the g -factor can be attributed to the enhanced mixing of electron bands with the split-off electron bands under a strong confinement regime as recently proposed for perovskite nanocrystals.⁶⁰

CONCLUSIONS

We studied the bright in-plane exciton FSS together with its g -factors for the PEA₂(MA) _{$n-1$} Pb _{n} I _{$3n+1$} compounds with n varying from 1 to 4. We have shown that similar to pure 2D and 3D cases, the in-plane excitonic states exhibit splitting and orthogonally oriented dipoles under the intermediate confinement regime. For the first time, we have described the evolution of the exciton g -factors as a function of n for PEA₂(MA) _{$n-1$} Pb _{n} I _{$3n+1$} . The observed FSS, together with the exciton g -factors, approaches the value characteristic of bulk metal-halide perovskite as n increases. The evolution of both quantities can be understood as a result of the decreasing confinement. The parameters provided form a solid basis for further studies of the band structure and excitons in lead-halide perovskites, in particular, the role of quantum and dielectric confinement.

EXPERIMENTAL METHODS

Synthesis and Sample Preparation. The synthesis of the samples was done using the cooling-induced crystallization method, described in detail in references 45 and 46.^{45,46} The high phase purity of these samples was confirmed by a powder X-ray diffraction technique using a Bruker D8 ADVANCE diffractometer.

Optical Measurements. For PL and reflectance measurements without the use of a magnetic field, the samples were mounted on the cold finger of a He flow optical cryostat. All of these measurements were performed at 4.2 K.

For the microreflectance measurements, white light was provided by a tungsten halogen light source by Ocean Optics. The excitation and signal collection were done by using a long working distance microscope objective with 50 \times magnification and an NA of 0.55. The optical signal was analyzed with a 500 mm long monochromator with a grating of 1800 grooves per mm and detected with a liquid-nitrogen-cooled CCD camera. We mounted a half-wave plate in the detection path of our setup, in front of a linear polarizer oriented along the preferred polarization of the spectrometer grating. Magnetorefectance measurements were performed at $T = 10$ K in a superconducting magnet in static magnetic fields up to 12 T. We used a 515 nm CW laser and a microscope objective with an NA of 0.82. The signal from the magnet was analyzed with a 750 mm long monochromator with a

grating of 1800 grooves per mm and detected with a liquid-nitrogen-cooled CCD camera.

ASSOCIATED CONTENT

Supporting Information

The Supporting Information is available free of charge at <https://pubs.acs.org/doi/10.1021/jacs.3c11957>.

Crystal photographs, X-ray diffraction patterns, discussion of PL and reflectance spectra interpretation, analysis of polarization-resolved reflectance spectra, and reflectance spectra measured in the magnetic field (PDF)

AUTHOR INFORMATION

Corresponding Authors

Michał Baranowski – Department of Experimental Physics, Faculty of Fundamental Problems of Technology, Wrocław University of Science and Technology, Wrocław 50-370, Poland; orcid.org/0000-0002-5974-0850; Email: michal.baranowski@pwr.edu.pl

Paulina Plochocka – Department of Experimental Physics, Faculty of Fundamental Problems of Technology, Wrocław University of Science and Technology, Wrocław 50-370, Poland; Laboratoire National des Champs Magnétiques Intenses, EMFL, CNRS UPR 3228, Université Grenoble Alpes, Université Toulouse, Université Toulouse 3, Toulouse 31400, France; orcid.org/0000-0002-4019-6138; Email: paulina.plochocka@lncmi.cnrs.fr

Authors

Katarzyna Posmyk – Department of Experimental Physics, Faculty of Fundamental Problems of Technology, Wrocław University of Science and Technology, Wrocław 50-370, Poland; Laboratoire National des Champs Magnétiques Intenses, EMFL, CNRS UPR 3228, Université Grenoble Alpes, Université Toulouse, Université Toulouse 3, Toulouse 31400, France; orcid.org/0000-0003-4655-5231

Natalia Zawadzka – Institute of Experimental Physics, Faculty of Physics, University of Warsaw, Warsaw 02-093, Poland; orcid.org/0000-0002-3282-9513

Lucja Kipczak – Institute of Experimental Physics, Faculty of Physics, University of Warsaw, Warsaw 02-093, Poland; orcid.org/0000-0003-1266-0201

Mateusz Dyksik – Department of Experimental Physics, Faculty of Fundamental Problems of Technology, Wrocław University of Science and Technology, Wrocław 50-370, Poland; orcid.org/0000-0003-4945-8795

Alessandro Surrente – Department of Experimental Physics, Faculty of Fundamental Problems of Technology, Wrocław University of Science and Technology, Wrocław 50-370, Poland; orcid.org/0000-0003-4078-4965

Duncan K. Maude – Laboratoire National des Champs Magnétiques Intenses, EMFL, CNRS UPR 3228, Université Grenoble Alpes, Université Toulouse, Université Toulouse 3, Toulouse 31400, France

Tomasz Kazimierzczuk – Institute of Experimental Physics, Faculty of Physics, University of Warsaw, Warsaw 02-093, Poland; orcid.org/0000-0001-6545-4167

Adam Babiński – Institute of Experimental Physics, Faculty of Physics, University of Warsaw, Warsaw 02-093, Poland

Maciej R. Molas – Institute of Experimental Physics, Faculty of Physics, University of Warsaw, Warsaw 02-093, Poland; orcid.org/0000-0002-5516-9415

Wakul Bumrungsan – Department of Materials Science and Engineering, School of Molecular Science and Engineering, Vidyasirimedhi Institute of Science and Technology (VISTEC), Rayong 21210, Thailand

Chanisara Chooseng – Department of Chemical and Biomolecular Engineering, School of Energy Science and Engineering, Vidyasirimedhi Institute of Science and Technology (VISTEC), Rayong 21210, Thailand

Watcharaphol Paritmongkol – Department of Chemical Engineering, Massachusetts Institute of Technology, Cambridge, Massachusetts 02139, United States; Department of Chemistry, Massachusetts Institute of Technology, Cambridge, Massachusetts 02139, United States; Department of Materials Science and Engineering, School of Molecular Science and Engineering, Vidyasirimedhi Institute of Science and Technology (VISTEC), Rayong 21210, Thailand; orcid.org/0000-0003-1638-6828

William A. Tisdale – Department of Chemical Engineering, Massachusetts Institute of Technology, Cambridge, Massachusetts 02139, United States; orcid.org/0000-0002-6615-5342

Complete contact information is available at:
<https://pubs.acs.org/10.1021/jacs.3c11957>

Notes

The authors declare no competing financial interest.

ACKNOWLEDGMENTS

This work has been partially funded by the National Science Centre, Poland, within the MAESTRO program grant no. 2020/38/A/ST3/00214 (P.P.). A.S. and K.P. appreciate the support of the National Science Centre, Poland, grant no. 2020/39/D/ST3/03000. M.D. acknowledges support from the National Science Centre, Poland, grant no. 2021/43/D/ST3/01444 and the Polish National Agency for Academic Exchange (grant no. BPN/BKK/2021/1/00002/U/00001). The Polish participation in the European Magnetic Field Laboratory (EMFL) is supported by the DIR/WK/2018/07 grant from the Ministry of Science and Higher Education, Poland. Work by W.P. and W.A.T. at MIT was supported by the U.S. Department of Energy, Office of Science, Basic Energy Sciences, under award number DE-SC0019345. Work by W.B., C.C., and W.P. at Vidyasirimedhi Institute of Science and Technology (VISTEC) was supported by VISTEC PhD scholarship and start-up funding. This study has been partially supported through the EUR grant NanoX no. ANR-17-EURE-0009 in the framework of the “Programme des Investissements d’Avenir”. The support from the National Science Centre, Poland, through grant nos. 2018/31/B/ST3/02111 (N.Z. and M.R.M.) and 2017/27/B/ST3/00205 (A.B. and T.K.) is acknowledged. The access to facilities was supported by the European Union’s Horizon 2020 research and innovation programme through the ISABEL project (no. 871106).

REFERENCES

(1) Bayer, M.; Ortner, G.; Stern, O.; Kuther, A.; Gorbunov, A.; Forchel, A.; Hawrylak, P.; Fafard, S.; Hinzer, K.; Reinecke, T.; et al. Fine structure of neutral and charged excitons in self-assembled In(Ga)As/(Al)GaAs quantum dots. *Phys. Rev. B* **2002**, *65*, 195315.

(2) Nestoklon, M.; Goupalov, S.; Dzhirov, R.; Ken, O.; Korenev, V.; Kusrayev, Y. G.; Sapega, V.; de Weerd, C.; Gomez, L.; Gregorkiewicz, T.; et al. Optical orientation and alignment of excitons in ensembles of inorganic perovskite nanocrystals. *Phys. Rev. B* **2018**, *97*, 235304.

(3) Posmyk, K.; Zawadzka, N.; Dyksik, M.; Surrente, A.; Maude, D. K.; Kazmierczuk, T.; Babinski, A.; Molas, M. R.; Paritmongkol, W.; Maczka, M.; Tisdale, W. A.; Plochocka, P.; Baranowski, M. Quantification of Exciton Fine Structure Splitting in a Two-Dimensional Perovskite Compound. *J. Phys. Chem. Lett.* **2022**, *13*, 4463–4469.

(4) Dyksik, M.; Duim, H.; Maude, D. K.; Baranowski, M.; Loi, M. A.; Plochocka, P. Brightening of dark excitons in 2D perovskites. *Sci. Adv.* **2021**, *7*, No. eabk0904.

(5) Quarti, C.; Giorgi, G.; Katan, C.; Even, J.; Palummo, M. Exciton ground state fine structure and excited states landscape in layered halide perovskites from combined BSE simulations and symmetry analysis. *Adv. Opt. Mater.* **2023**, 2202801.

(6) Do, T. T. H.; Granados del Aguila, A.; Zhang, D.; Xing, J.; Liu, S.; Prosnikov, M.; Gao, W.; Chang, K.; Christianen, P. C.; Xiong, Q. Bright exciton fine-structure in two-dimensional lead halide perovskites. *Nano Lett.* **2020**, *20*, 5141–5148.

(7) Fu, M.; Tamarat, P.; Huang, H.; Even, J.; Rogach, A. L.; Lounis, B. Neutral and charged exciton fine structure in single lead halide perovskite nanocrystals revealed by magneto-optical spectroscopy. *Nano Lett.* **2017**, *17*, 2895–2901.

(8) Kim, J.; Wong, C. Y.; Scholes, G. D. Exciton fine structure and spin relaxation in semiconductor colloidal quantum dots. *Acc. Chem. Res.* **2009**, *42*, 1037–1046.

(9) Leo, K.; Shah, J.; Göbel, E. O.; Damen, T. C.; Schmitt-Rink, S.; Schäfer, W.; Köhler, K. Coherent oscillations of a wave packet in a semiconductor double-quantum-well structure. *Phys. Rev. Lett.* **1991**, *66*, 201–204.

(10) Kheng, K.; Cox, R.; d’Aubigné, M. Y.; Bassani, F.; Saminadayar, K.; Tatarenko, S. Observation of negatively charged excitons X⁻ in semiconductor quantum wells. *Phys. Rev. Lett.* **1993**, *71*, 1752–1755.

(11) Blackwood, E.; Snelling, M.; Harley, R.; Andrews, S.; Foxon, C. Exchange interaction of excitons in GaAs heterostructures. *Phys. Rev. B* **1994**, *50*, 14246–14254.

(12) Han, Y.; Liang, W.; Lin, X.; Li, Y.; Sun, F.; Zhang, F.; Sercel, P. C.; Wu, K. Lattice distortion inducing exciton splitting and coherent quantum beating in CsPbI₃ perovskite quantum dots. *Nat. Mater.* **2022**, *21*, 1282–1289.

(13) Wang, G.; Chernikov, A.; Glazov, M. M.; Heinz, T. F.; Marie, X.; Amand, T.; Urbaszek, B. Colloquium: Excitons in atomically thin transition metal dichalcogenides. *Rev. Mod. Phys.* **2018**, *90*, 021001.

(14) Straus, D. B.; Kagan, C. R. Electrons, excitons, and phonons in two-dimensional hybrid perovskites: connecting structural, optical, and electronic properties. *J. Phys. Chem. Lett.* **2018**, *9*, 1434–1447.

(15) Aslan, B.; Chenet, D. A.; Van Der Zande, A. M.; Hone, J. C.; Heinz, T. F. Linearly polarized excitons in single- and few-layer ReS₂ crystals. *ACS Photonics* **2016**, *3*, 96–101.

(16) Wang, X.; Jones, A. M.; Seyler, K. L.; Tran, V.; Jia, Y.; Zhao, H.; Wang, H.; Yang, L.; Xu, X.; Xia, F. Highly anisotropic and robust excitons in monolayer black phosphorus. *Nat. Nanotechnol.* **2015**, *10*, 517–521.

(17) Chen, Y.; Sun, Y.; Peng, J.; Tang, J.; Zheng, K.; Liang, Z. 2D Ruddlesden–Popper perovskites for optoelectronics. *Adv. Mater.* **2018**, *30*, 1703487.

(18) Blancon, J.-C.; Stier, A. V.; Tsai, H.; Nie, W.; Stoumpos, C. C.; Traore, B.; Pedesseau, L.; Kepenekian, M.; Katsutani, F.; Noe, G.; et al. Scaling law for excitons in 2D perovskite quantum wells. *Nat. Commun.* **2018**, *9*, 2254.

(19) Wang, J.; Su, R.; Xing, J.; Bao, D.; Diederichs, C.; Liu, S.; Liew, T. C.; Chen, Z.; Xiong, Q. Room temperature coherently coupled exciton–polaritons in two-dimensional organic–inorganic perovskite. *ACS Nano* **2018**, *12*, 8382–8389.

(20) Su, R.; Fieramosca, A.; Zhang, Q.; Nguyen, H. S.; Deleporte, E.; Chen, Z.; Sanvitto, D.; Liew, T. C.; Xiong, Q. Perovskite semiconductors for room-temperature exciton-polaritons. *Nat. Mater.* **2021**, *20*, 1315–1324.

(21) Dyksik, M.; Duim, H.; Zhu, X.; Yang, Z.; Gen, M.; Kohama, Y.; Adjoktse, S.; Maude, D. K.; Loi, M. A.; Egger, D. A.; et al. Broad

Tunability of Carrier Effective Masses in Two-Dimensional Halide Perovskites. *ACS Energy Lett.* **2020**, *5*, 3609–3616.

(22) Canet-Albiach, R.; Krecmarova, M.; Bailach, J. B.; Gualdrón-Reyes, A. F.; Rodríguez-Romero, J.; Gorji, S.; Pashaei-Adl, H.; Mora-Seró, I.; Martínez Pastor, J. P.; Sánchez-Royo, J. F.; et al. Revealing Giant Exciton Fine-Structure Splitting in Two-Dimensional Perovskites Using van der Waals Passivation. *Nano Lett.* **2022**, *22*, 7621–7627.

(23) Baranowski, M.; Galkowski, K.; Surrente, A.; Urban, J.; Kłopotowski, Ł.; Mackowski, S.; Maude, D. K.; Ben Aich, R.; Boujdaria, K.; Chamarro, M.; et al. Giant Fine Structure Splitting of the Bright Exciton in a Bulk MAPbBr₃ Single Crystal. *Nano Lett.* **2019**, *19*, 7054–7061.

(24) Posmyk, K.; Dyksik, M.; Surrente, A.; Maude, D. K.; Zawadzka, N.; Babinski, A.; Molas, M. R.; Paritmongkol, W.; Maczka, M.; Tisdale, W. A.; Plochocka, P.; Baranowski, M. Exciton Fine Structure in 2D Perovskites: The Out-of-Plane Excitonic State. *Adv. Opt. Mater.* **2023**, *2300877*.

(25) Gramlich, M.; Swift, M. W.; Lampe, C.; Lyons, J. L.; Döblinger, M.; Efros, A. L.; Sercel, P. C.; Urban, A. S. Dark and Bright Excitons in Halide Perovskite Nanoplatelets. *Advanced Science* **2022**, *9*, 2103013.

(26) Fu, H.; Wang, L.-W.; Zunger, A. Excitonic exchange splitting in bulk semiconductors. *Phys. Rev. B* **1999**, *59*, 5568–5574.

(27) Fang, H.-H.; Yang, J.; Adjokatsé, S.; Tekelenburg, E.; Kamminga, M. E.; Duim, H.; Ye, J.; Blake, G. R.; Even, J.; Loi, M. A. Band-edge exciton fine structure and exciton recombination dynamics in single crystals of layered hybrid perovskites. *Adv. Funct. Mater.* **2020**, *30*, 1907979.

(28) Folpini, G.; Cortecchia, D.; Petrozza, A.; Srimath Kandada, A. R. The role of a dark exciton reservoir in the luminescence efficiency of two-dimensional tin iodide perovskites. *J. Mater. Chem. C* **2020**, *8*, 10889–10896.

(29) Posmyk, K.; Dyksik, M.; Surrente, A.; Zalewska, K.; Śmiertka, M.; Cybula, E.; Paritmongkol, W.; Tisdale, W. A.; Plochocka, P.; Baranowski, M. Fine Structure Splitting of Phonon-Assisted Excitonic Transition in (PEA)₂PbI₄ Two-Dimensional Perovskites. *Nanomaterials* **2023**, *13*, 1119.

(30) Senellart, P.; Solomon, G.; White, A. High-performance semiconductor quantum-dot single-photon sources. *Nat. Nanotechnol.* **2017**, *12*, 1026–1039.

(31) Stevenson, R. M.; Young, R. J.; Atkinson, P.; Cooper, K.; Ritchie, D. A.; Shields, A. J. A semiconductor source of triggered entangled photon pairs. *Nature* **2006**, *439*, 179–182.

(32) Cai, R.; Wadgaonkar, I.; Lim, J. W. M.; Dal Forno, S.; Giovanni, D.; Feng, M.; Ye, S.; Battiatto, M.; Sum, T. C. Zero-field quantum beats and spin decoherence mechanisms in CsPbBr₃ perovskite nanocrystals. *Nat. Commun.* **2023**, *14*, 2472.

(33) Even, J.; Pedesseau, L.; Katan, C. Understanding quantum confinement of charge carriers in layered 2D hybrid perovskites. *ChemPhysChem* **2014**, *15*, 3733–3741.

(34) Hong, X.; Ishihara, T.; Nurmikko, A. Dielectric confinement effect on excitons in PbI₄-based layered semiconductors. *Phys. Rev. B* **1992**, *45*, 6961–6964.

(35) Dyksik, M.; Wang, S.; Paritmongkol, W.; Maude, D. K.; Tisdale, W. A.; Baranowski, M.; Plochocka, P. Tuning the Excitonic Properties of the 2D (PEA)₂(MA)_{n-1}Pb_nI_{3n+1} Perovskite Family via Quantum Confinement. *J. Phys. Chem. Lett.* **2021**, *12*, 1638–1643.

(36) Surrente, A.; Baranowski, M.; Plochocka, P. Perspective on the physics of two-dimensional perovskites in high magnetic field. *Appl. Phys. Lett.* **2021**, *118*, 170501.

(37) Baranowski, M.; Plochocka, P. Excitons in metal-halide perovskites. *Adv. Energy Mater.* **2020**, *10*, 1903659.

(38) Tamarat, P.; Bodnarchuk, M. I.; Trebbia, J.-B.; Erni, R.; Kovalenko, M. V.; Even, J.; Lounis, B. The ground exciton state of formamidinium lead bromide perovskite nanocrystals is a singlet dark state. *Nat. Mater.* **2019**, *18*, 717–724.

(39) Kataoka, T.; Kondo, T.; Ito, R.; Sasaki, S.; Uchida, K.; Miura, N. Magneto-optical study on the excitonic spectrum of (C₆H₁₃NH₃)₂PbI₄. *Phys. B* **1993**, *184*, 132–136.

(40) Tanaka, K.; Takahashi, T.; Kondo, T.; Umeda, K.; Ema, K.; Umabayashi, T.; Asai, K.; Uchida, K.; Miura, N. Electronic and excitonic structures of inorganic–organic perovskite-type quantum-well crystal (C₄H₉NH₃)₂PbBr₄. *Jpn. J. Appl. Phys.* **2005**, *44*, 5923.

(41) Yu, Z. Effective-mass model and magneto-optical properties in hybrid perovskites. *Sci. Rep.* **2016**, *6* (1), 28576.

(42) Ramade, J.; Andriambarijaona, L. M.; Steinmetz, V.; Goubet, N.; Legrand, L.; Barisien, T.; Bernardot, F.; Testelin, C.; Lhuillier, E.; Bramati, A.; et al. Fine structure of excitons and electron–hole exchange energy in polymorphic CsPbBr₃ single nanocrystals. *Nanoscale* **2018**, *10*, 6393–6401.

(43) Yin, C.; Chen, L.; Song, N.; Lv, Y.; Hu, F.; Sun, C.; Yu, W. W.; Zhang, C.; Wang, X.; Zhang, Y.; et al. Bright-Exciton Fine-Structure Splittings in Single Perovskite Nanocrystals. *Phys. Rev. Lett.* **2017**, *119*, 026401.

(44) Becker, M. A.; Vaxenburg, R.; Nedelcu, G.; Sercel, P. C.; Shabaev, A.; Mehl, M. J.; Michopoulos, J. G.; Lambrakos, S. G.; Bernstein, N.; Lyons, J. L.; et al. Bright triplet excitons in caesium lead halide perovskites. *Nature* **2018**, *553*, 189–193.

(45) Paritmongkol, W.; Dahod, N. S.; Stollmann, A.; Mao, N.; Settens, C.; Zheng, S.-L.; Tisdale, W. A. Synthetic variation and structural trends in layered two-dimensional alkylammonium lead halide perovskites. *Chem. Mater.* **2019**, *31*, 5592–5607.

(46) Paritmongkol, W.; Powers, E. R.; Dahod, N. S.; Tisdale, W. A. Two origins of broadband emission in multilayered 2D lead iodide perovskites. *J. Phys. Chem. Lett.* **2020**, *11*, 8565–8572.

(47) Jin, H.; Debroye, E.; Keshavarz, M.; Scheblykin, I. G.; Roeyfaers, M. B.; Hofkens, J.; Steele, J. A. It's a trap! On the nature of localised states and charge trapping in lead halide perovskites. *Mater. Horiz.* **2020**, *7*, 397–410.

(48) Zuri, S.; Shapiro, A.; Kronik, L.; Lifshitz, E. Uncovering Multiple Intrinsic Chiral Phases in (PEA)₂PbI₄ Halide Perovskites. *J. Phys. Chem. Lett.* **2023**, *14*, 4901–4907.

(49) Dar, M. I.; Jacopin, G.; Meloni, S.; Mattoni, A.; Arora, N.; Boziki, A.; Zakeeruddin, S. M.; Rothlisberger, U.; Grätzel, M. Origin of unusual bandgap shift and dual emission in organic-inorganic lead halide perovskites. *Sci. Adv.* **2016**, *2*, No. e1601156.

(50) Tao, W.; Zhang, C.; Zhou, Q.; Zhao, Y.; Zhu, H. Momentarily trapped exciton polaron in two-dimensional lead halide perovskites. *Nat. Commun.* **2021**, *12*, 1400.

(51) Kahmann, S.; Duim, H.; Fang, H.-H.; Dyksik, M.; Adjokatsé, S.; Rivera Medina, M.; Pitaro, M.; Plochocka, P.; Loi, M. A. Photophysics of two-dimensional perovskites—learning from metal halide substitution. *Adv. Funct. Mater.* **2021**, *31*, 2103778.

(52) Wright, A. D.; Milot, R. L.; Eperon, G. E.; Snaith, H. J.; Johnston, M. B.; Herz, L. M. Band-tail recombination in hybrid lead iodide perovskite. *Adv. Funct. Mater.* **2017**, *27*, 1700860.

(53) Baranowski, M.; Urban, J. M.; Zhang, N.; Surrente, A.; Maude, D.; Andaji-Garmaroudi, Z.; Stranks, S.; Plochocka, P. Static and dynamic disorder in triple-cation hybrid perovskites. *J. Phys. Chem. C* **2018**, *122*, 17473–17480.

(54) Hurtado Parra, S.; Straus, D. B.; Fichera, B. T.; Iotov, N.; Kagan, C. R.; Kikkawa, J. M. Large exciton polaron formation in 2D hybrid perovskites via time-resolved photoluminescence. *ACS Nano* **2022**, *16*, 21259–21265.

(55) Baranowski, M.; Zelewski, S. J.; Kepenekian, M.; Traoré, B.; Urban, J. M.; Surrente, A.; Galkowski, K.; Maude, D. K.; Kuc, A.; Booker, E. P.; et al. Phase-Transition-Induced Carrier Mass Enhancement in 2D Ruddlesden–Popper Perovskites. *ACS Energy Lett.* **2019**, *4*, 2386–2392.

(56) Guilloux, V.; Ghribi, A.; Majrab, S.; Margailan, F.; Bernard, M.; Bernardot, F.; Legrand, L.; Lhuillier, E.; Boujdaria, K.; Chamarro, M.; et al. Exciton Fine Structure of CsPbCl₃ Nanocrystals: An Interplay of Electron–Hole Exchange Interaction, Crystal Structure, Shape Anisotropy, and Dielectric Mismatch. *ACS Nano* **2023**, *17*, 12266–12277.

(57) Urban, J. M.; Chehade, G.; Dyksik, M.; Menahem, M.; Surrente, A.; Trippé-Allard, G.; Maude, D. K.; Garrot, D.; Yaffe, O.; Deleporte, E.; et al. Revealing Excitonic Phonon Coupling in $(\text{PEA})_2(\text{MA})_{n-1}\text{Pb}_n\text{I}_{3n+1}$ 2D Layered Perovskites. *J. Phys. Chem. Lett.* **2020**, *11*, 5830–5835.

(58) Kirstein, E.; Yakovlev, D. R.; Glazov, M. M.; Zhukov, E. A.; Kudlacik, D.; Kalitukha, I. V.; Sapega, V. F.; Dimitriev, G. S.; Semina, M. A.; Nestoklon, M. O.; et al. The Landé factors of electrons and holes in lead halide perovskites: universal dependence on the band gap. *Nat. Commun.* **2022**, *13*, 3062.

(59) Miura, N. *Physics of Semiconductors in High Magnetic Fields*; OUP Oxford, 2007; Vol. 15.

(60) Nestoklon, M. O.; Kirstein, E.; Yakovlev, D. R.; Zhukov, E. A.; Glazov, M. M.; Semina, M. A.; Ivchenko, E. L.; Kolobkova, E. V.; Kuznetsova, M. S.; Bayer, M. Tailoring the electron and hole Landé factors in lead halide perovskite nanocrystals by quantum confinement and halide exchange. *Nano Lett.* **2023**, *23*, 8218–8224.

(61) Kirstein, E.; Zhukov, E. A.; Yakovlev, D. R.; Kopteva, N. E.; Harkort, C.; Kudlacik, D.; Hordiichuk, O.; Kovalenko, M. V.; Bayer, M. Coherent Spin Dynamics of Electrons in Two-Dimensional (PEA) 2PbI_4 Perovskites. *Nano Lett.* **2023**, *23*, 205–212.

(62) Harkort, C.; Kudlacik, D.; Kopteva, N. E.; Yakovlev, D. R.; Karzel, M.; Kirstein, E.; Hordiichuk, O.; Kovalenko, M. V.; Bayer, M. Spin-Flip Raman Scattering on Electrons and Holes in Two-Dimensional (PEA) 2PbI_4 Perovskites. *Small* **2023**, *19*, 2300988.



CAS BIOFINDER DISCOVERY PLATFORM™

ELIMINATE DATA SILOS. FIND WHAT YOU NEED, WHEN YOU NEED IT.

A single platform for relevant, high-quality biological and toxicology research

Streamline your R&D

CAS
A division of the American Chemical Society